Analysis of the efficiency of intensity measures from real earthquake data recorded in buildings

Article *in* Soil Dynamics and Earthquake Engineering · May 2021

DOI: 10.1016/j.soildyn.2021.106751

3 authors:

Subash Ghimire
University of Grenoble
6 PUBLICATIONS **48** CITATIONS
SEE PROFILE

Philippe Gueguen
Université Gustave Eiffel/Université Grenoble Alpes
248 PUBLICATIONS **4,771** CITATIONS
SEE PROFILE

Ariana Astorga
Université Grenoble Alpes
19 PUBLICATIONS **107** CITATIONS
SEE PROFILE

Soil Dynamics and Earthquake Engineering xxx (xxxx) xxx

Contents lists available at ScienceDirect

Soil Dynamics and Earthquake Engineering

journal homepage: www.elsevier.com/locate/soildyn

Analysis of the efficiency of intensity measures from real earthquake data recorded in buildings

Subash Ghimire *, Philippe Guéguen, Ariana Astorga

ISTerre, Université Grenoble Alpes, CNRS/USMB/IRD/UGE, Grenoble, France

ARTICLE INFO

Keywords:
Structural performance assessment
Strong motion recordings in buildings
Building frequency
Efficiency and sufficiency of IM

ABSTRACT

In this paper, a number of spectral and ordinary ground motion intensity measures (IMs) are tested for use in structural performance assessment. Real strong motion values recorded at the top and the bottom of US, Japanese and Romanian buildings are analyzed in order to identify the source of uncertainties in the prediction of engineering demand parameters (i.e. structural drift) for given IMs (i.e. $\sigma_{EDP|IM}$). The efficiency and sufficiency of each IM from a large set of building and earthquake motion data are tested for different criteria characterizing the seismic source (magnitude and source-to-site distance), and considering several building classes and a specific single-building analysis including aging due to cumulative earthquake damage over time. The spectral values at co-seismic resonance frequencies was found to be the most efficient IMs for the range of buildings and earthquakes investigated, particularly for velocity with a reduction of approximately 50% of the $\sigma_{EDP|IM}$ value. Conversely, most IMs are relatively insufficient.

1. Introduction

Performance-based earthquake engineering (PBEE) refers to the probabilistic framework in which earthquake consequences are expressed by a set of performance objectives, based on a comprehensive scientific foundation [1]. Depending on the application, these performance objectives can help stakeholders to make decisions with regard to crisis management and structural capacity, such as immediate occupancy or near-collapse levels, by predicting human or economic losses. In the framework proposed by PEER [1], PBEE works in four stages, starting with the hazard itself through to the consequence analysis. In hazard analysis, intensity measures (IM) and their annual frequency of exceedance (λ_{IM}) are defined by probabilistic seismic hazard assessment (PSHA). In structural analysis, the response of the structure to a given IM can be modeled and expressed in terms of engineering demand parameters (EDPs), such as structural drift, maximal top acceleration, etc. In damage analysis, damage measurement (DM) is calculated based on EDP values and models of structure capacity or fragility. Finally, the earthquake's consequences, in terms of repair costs, operability of the structure and potential economic or human losses for a given DM, can be calculated and expressed as decision variables (DVs) on which stakeholders can base their decisions in view of the expected performance levels.

The four steps of the underlying probabilistic framework of PBEE estimate the frequency of failure of a performance level over a given period of time; this involves uncertainties. For example, the annual frequency of exceeding a given EDP value (λ_{EDP}) is expressed by:

$$\lambda_{EDP} = \int_{im} P[EDP / IM = im] \left| d\lambda_{im} \right| \quad (1)$$

where P(EDP|IM = im) is the conditional probability of occurrence of each EDP value, taking into account the value of the IM, and $d\lambda_{im}$ is the annual rate of exceeding an IM value, derived from the hazard curves. P(EDP|IM = im) is usually obtained by considering a series of nonlinear dynamic analyses of the structure. Baker and Cornell [2] provide a detailed description of approaches to characterize and propagate uncertainties at each step. Current research on PBEE is mainly focused on identifying the origins of uncertainties, distinguishing between epistemic and random uncertainties, in order to boost scientific efforts on the reducible elements that contribute most to performance uncertainty (e.g. Ref. [3]). In practice, P(EDP|IM = im) satisfies a chosen model of EDP distribution for a given IM and is obtained by regression of EDP values for IM values. Luco [4], Luco and Cornell [5], and Baker and Cornell [6] considered an IM to be sufficient if the prediction of EDP given IM is statistically independent of earthquake magnitude and

* Corresponding author. ISTerre, CS40700, 38058, Grenoble cedex 9, France.
E-mail address: subash.ghimire@univ-grenoble-alpes.fr (S. Ghimire).

https://doi.org/10.1016/j.soildyn.2021.106751
Received 4 June 2020; Received in revised form 1 March 2021; Accepted 31 March 2021

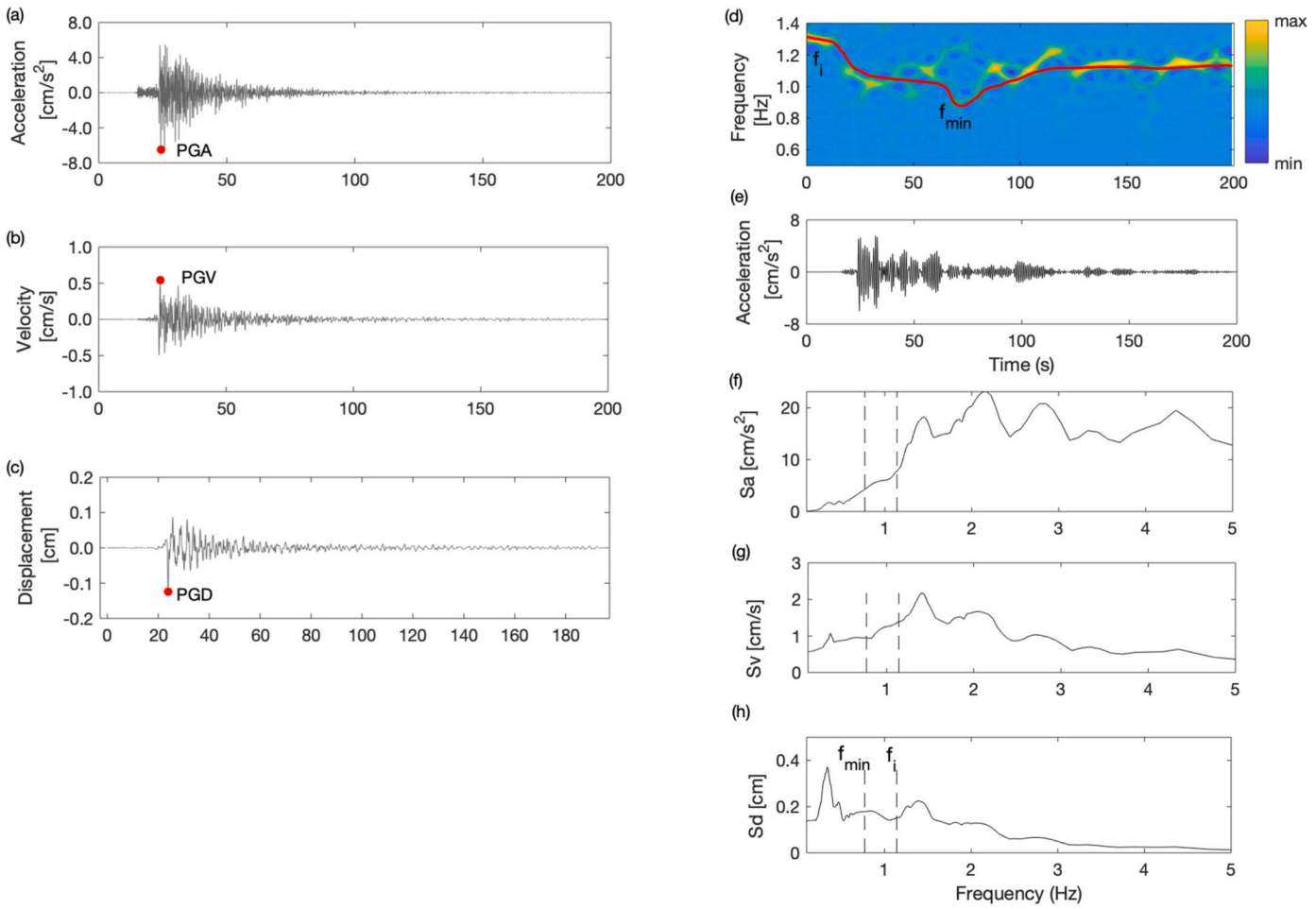

Fig. 1. Illustrations on the left side is the time history of (a) acceleration, (b) velocity, (c) displacement, recorded at the bottom floor sensor of the building. The red dots (a–c) correspond to the peak values. Similarly, the figures on the right side are (d) the pseudo-Wigner-Ville time-frequency distribution, the red-line is the smoothing of the maximum of Wigner-Ville, (e) the acceleration recorded at the top floor sensors. Response spectrum of (f) acceleration, (g) velocity, and (h) displacement, the dashed vertical line represents the position of elastic frequency (f_i) and co-seismic resonance frequency (f_{min}). (For interpretation of the references to colour in this figure legend, the reader is referred to the Web version of this article.)

epicentral distance values. Furthermore, the efficiency of IMs is assessed by measuring the variability of values of EDP (given IM) around the regression on the IM values. In general, Peak Ground Acceleration (PGA) or the acceleration spectral value at the resonance period T1 of the structure Sa(T1) (with 5% damping) are considered as outputs of the seismic hazard curves.

Structure response and the associated uncertainties are conditioned by time-history seismic excitation, considering the IM at which the EDP value is exceeded. The efficiency and sufficiency of Sa(T1) compared with PGA were investigated by Shome and Cornell [7] according to the type of building and the contribution of the higher modes to the total response was also considered [7]. Other ground motion parameters have also been investigated in terms of sufficiency and efficiency, such as peak values in velocity, duration or energy, or spectral values considering different resonant periods [8,9], spectral values in acceleration [5,7,10–12] or velocity [13,14], or by combining IMs based on vector-valued approach [6,15,16]. All these studies are based on the numerical modeling of structures considering different ground motion datasets, mostly using the Incremental Dynamic Analysis approach (IDA). In structural analysis, the selection or generation of natural or synthetic accelerograms from different tectonic areas, the scaling applied to obtain the desired structural response values, the selection of physical modal parameters (e.g., structural period and damping) and their co-seismic variations, as well as other modeling assumptions related to component fragility functions, affect the overall uncertainty of the performance estimate. Furthermore, a typical assumption in the assessment of P(EDP|IM) is that the building response variability for a class of buildings is the same as the response variability for a given building in this class (this assumption is an ergodic assumption affecting fragility curves).

According to several authors (e.g. Refs. [17,18]), considering that data from full-scale observations in real buildings are much more representative than even the most sophisticated laboratory or numerical experiments, one way of improving engineering science to understand the physical behavior of structures is to use a complete database of earthquake recordings in real structures. For example, Perrault and Guéguen [19] analyzed the variability of EDP versus IM using accelerometric data recorded in Californian buildings, taking structural drift as the EDP, and derived a single-building damage prediction equation (BDPE) with its associated uncertainties. Astorga et al. [20–22] completed the analysis, confirming the added value of physical data in understanding the seismic response of Japanese buildings in terms of co-seismic demand parameters related to modal (i.e. resonance frequency) parameter variations, especially during repetitive earthquake sequences.

In this study, the efficiency and sufficiency of several IMs for P(EDP|IM) from a large number of experimental datasets are analyzed using the regression model of EDP values for IM values. In the second section, the IMs and EDPs are described based on the study by Astorga et al. [22]. The third section describes the datasets and the methodology used.

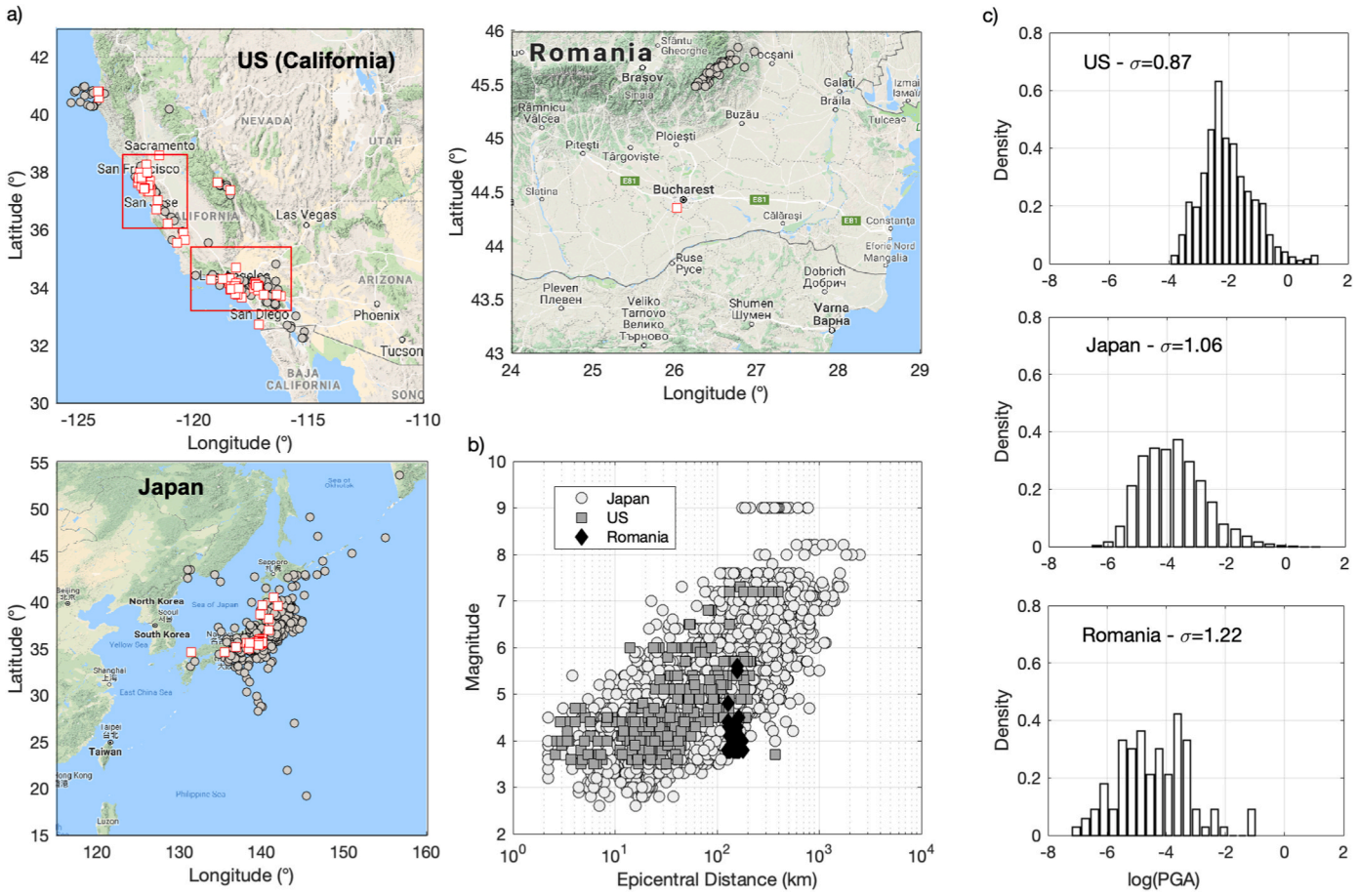

Fig. 2. View of the whole dataset used in this study. a) Positions of epicenters (gray circles) and buildings (red squares) in the US (California), Romania and Japan. For the US dataset, the two red rectangular boxes define the area of the two specific regions discussed in the manuscript. (b) Magnitude versus epicentral distance distribution of the whole dataset including Japan (open circles), the US (gray squares) and Romania (solid diamonds). (c) Distribution of natural log (PGA) for American, Japanese and Romanian datasets, respectively. σ is the standard deviation of the distribution. (For interpretation of the references to colour in this figure legend, the reader is referred to the Web version of this article.)

Then, the results in terms of efficiency and sufficiency are discussed in the fourth section, completed in the fifth by a specific analysis of the co-seismic frequency value versus EDP. Finally, the conclusion develops a simple empirical BDPE using available experimental data.

2. Description of IMs and EDPs

This study uses accelerometric data recorded in several sets of buildings and processed by Astorga et al. [22] for NDE1.0. Herein, we propose a brief description of the building information and earthquake data; more detailed information is available in NDE1.0 [22].

Six ordinary IM values are considered in this study, computed from the data recorded at the bottom floor of each building:

- Peak ground acceleration (PGA) (Fig. 1a), velocity (PGV) (Fig. 1b), and displacement (PGD) (Fig. 1c), corresponding to the absolute values of maximum acceleration, velocity and displacement time histories, respectively.
- Arias intensity (AI), destructive potential (DP) and cumulative absolute velocity (CAV). Arias intensity [23] includes both the amplitude and duration of seismic shaking, computed as follows:

$$AI = \frac{\pi}{2g}\int_0^{tf} a^2(t)dt \tag{2}$$

where g is the acceleration due to gravity, $a(t)$ is the acceleration recorded at time t, and t_f is the total duration of the recording. AI is an energy-based parameter that considers amplitude and duration of the ground motion, but it is unable to capture the frequency characteristics of ground motions. To overcome this, Araya and Saragoni [24] define DP, as follows:

$$DP = \frac{AI}{{v_0}^2} \tag{3}$$

where ${v_0}^2$ is the intensity of zero crossings, calculated over the entire duration of ground motion, as defined in its original version. Araya and Saragoni [24] have shown a strong correlation between DP and observed real damage. Actually, ${v_0}^2$ provides a measure of the dominant frequency content of the seismic ground motion.

Finally, Cumulative absolute velocity [25] is computed as follows:

$$CAV = \int_0^{tf} |a(t)|dt \tag{4}$$

where |a(t)| is the absolute value of acceleration at time t.

Six spectral IM values are also considered: spectral acceleration (5% damping) (SA_i and SA_{min}) (Fig. 1f), velocity (SV_i and SV_{min}) (Fig. 1g) and displacement (SD_i and SD_{min}) (Fig. 1h) for two specific frequency values (i and min) impacting seismic demand. Index i corresponds to the spectral value computed at the elastic frequency of the system f_i, i.e., the frequency obtained by Fourier analysis of the pre-event noise window

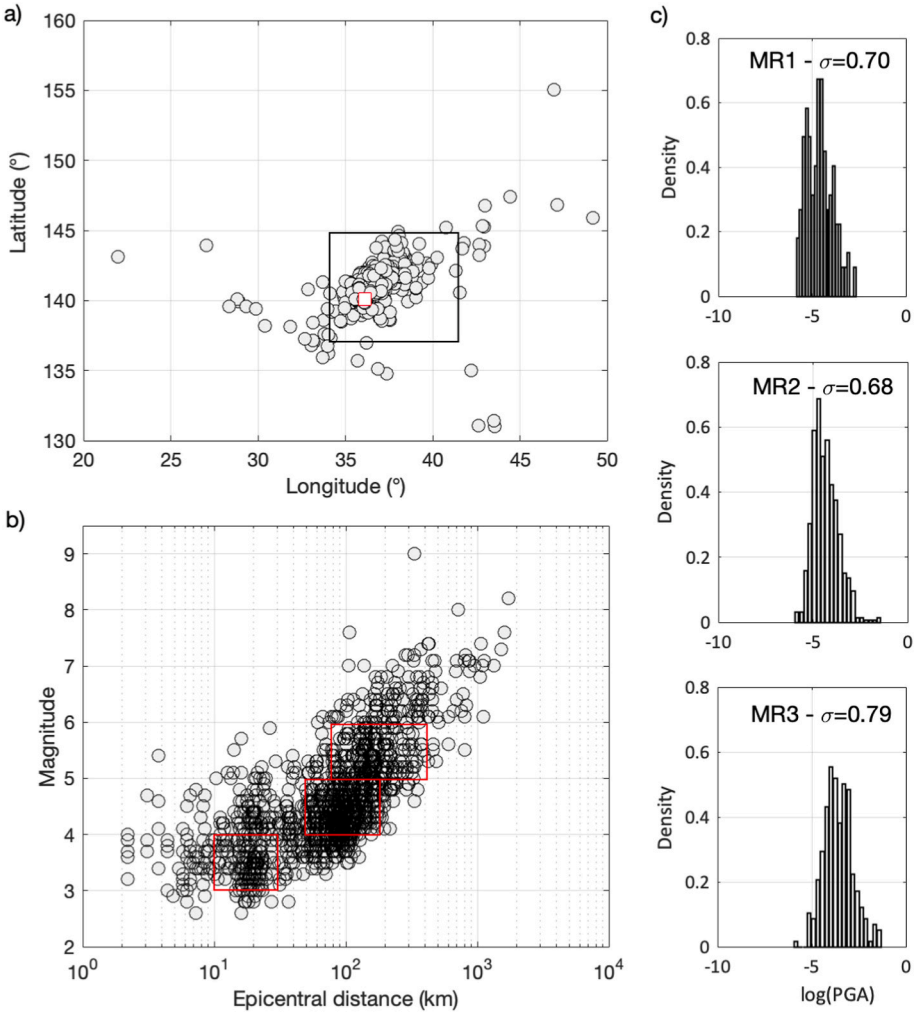

Fig. 3. Dataset for the specific Annex (ANX) building in Japan. (a) Location of the ANX building (red square) and related earthquake epicenters (gray circles). The black square represents the specific subset of data considered. (b) Magnitude versus epicentral distance distribution. The red rectangles define the boundaries of the three magnitude-distance criteria (MR1, MR2 and MR3) described herein. (c) Distribution of log (PGA) for specific magnitude-distance criteria MR1, MR2 and MR3. σ is the standard deviation of the distribution. (For interpretation of the references to colour in this figure legend, the reader is referred to the Web version of this article.)

before the earthquake. Index min corresponds to the minimal co-seismic value of the resonance frequency f_{min} during the strongest loading and obtained by applying a time-frequency distribution to the seismic recording (Fig. 1d), using the reassigned smoothed Wigner-Ville distribution [26]. The time-frequency distribution is applied to the top accelerometric time history (Fig. 1e). The time and frequency smoothing windows are Hamming windows, with N/10 and N/4 points, respectively. Then, a 3rd order Savitzky-Golay filter is applied to the maximum values of energy window. Fig. 1d shows an example of the time-frequency process applied to the data. The f_{min} corresponds to the average value of ±10 samples around the minimum value observed in the smoothing function [20].

Finally, in this study, drift ratio (DR) is considered as an EDP to describe the building response [22]. DR corresponds to the peak of the transient drift observed during the ground motion, obtained by computing the maximum relative displacement, as follows:

$$DR = \frac{\Delta_{top} - \Delta_{bottom}}{h} \quad (5)$$

where Δ_{top} and Δ_{bottom} are the horizontal displacements recorded at the top and bottom floors of each building, respectively, and h is the height between the top and bottom floors.

3. Data and methodology used

NDE1.0 accelerometric data [22] from the US and Japan plus additional data collected from Romania, processed according the same method as that defined in NDE1.0, were used in this study (Fig. 2). Information such as magnitude and epicentral distance is available for each earthquake but there is no description of the source parameters. A brief description of the buildings, earthquakes and datasets is given hereafter.

US data - Data from 84 US buildings provided by Center for Engineering Strong Motion Data (CESMD) (https://strongmotioncenter.org/) were considered (Fig. 2a). The distribution of the buildings according to construction material is as follows: 27% reinforced concrete (US-RC), 57% steel (US-ST), 11% masonry (US-MA), and 5% wood (US-WO). 684 accelerometric recordings were collected; among them, 225/302/134/24 recordings were collected from concrete/steel/masonry/wooden buildings. Moment magnitude (M_w) varies from 3.5 to 7.3 and epicentral distance varies from 2.6 to 331 km (Fig. 2b). The dataset includes strong earthquakes, such as the 7.2 M_w Landers event in 1992 and the 7.3 M_w Baja California event in 2010. Two subsets of Californian data are considered to assess uncertainties related to the tectonic context. These subsets are named specific tectonic source STS1 and STS2. The latitude and longitude boundaries of STS1 and STS2 are 33–35 and 35–39°; 116 to 120 and 120–123°, respectively (Fig. 2a).

RO data - A ten-story reinforced concrete building monitored by the National Center for Seismic Risk Reduction (NCSRR) of Romania is also considered. This building has been monitored since December 2013. 108 accelerometric records were collected, most of them corresponding to earthquakes located in the Vrancea seismic zone to the north of Bucharest (Fig. 2a). Epicentral distance thus varies slightly, between 127 and 178.3 km for M_w ranging from 3.8 to 5.6 (Fig. 2b). The largest

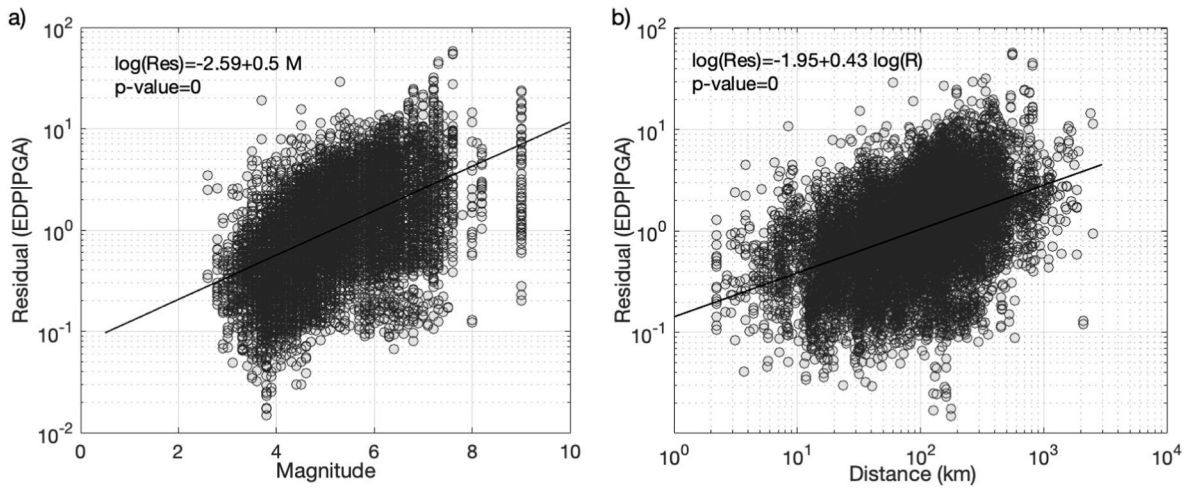

Fig. 4. Distribution of residual values (EDP|PGA) as function of (a) M and (b) log(R), considering the whole dataset. The lines represent the fitted linear model between log(R)/M and the residuals.

earthquakes M_w 5.6 and 5.4 in 2016 and 2014, respectively, are included.

JPN data – 11,763 accelerometric recordings from 32 high/mid-rise Japanese buildings were collected from the BRI strong motion network (https://smo.kenken.go.jp/) (Fig. 2a). The building distribution according to elementary typology is as follows: 24% steel (JPN-ST), 40% reinforced concrete (JPN-RC), and 36% steel-reinforced concrete (JPN-SRC). The main shock and aftershock sequences of the strongest earthquake, 2011 Tohuku, are included. Magnitude varies from 2.6 to 9.1 (JMA magnitude) and epicentral distance varies from 2.2 to 2394 km (Fig. 2b).

ANX – One of the Japanese buildings, ANX, is a building that has been studied extensively by the BRI strong motion network. A detailed description of ANX is available in Astorga et al. [20]. ANX is an 8-story, steel-reinforced concrete building located approximately 60 km northwest of Tokyo, in Tsukuba (Japan) (Fig. 3a). ANX has one basement floor resting on spread foundations (8.2 m deep) lying on soft soil made up of alternating layers of clay and sandy-clay to a depth of 40 m. A description of the instrumentation is provided by Kashima [27,28]. The ANX dataset is the largest of our datasets, comprising 1630 recordings in both horizontal directions, made over a period of 20 years, starting immediately after building completion in March 1998 and including the main shock and aftershocks of the 2011 Tohuku earthquake. Magnitude varies from 2.6 to 9.1 and epicentral distance varies from 2.2 to 1730 km. (Fig. 3b). A specific subset of data for ANX is considered, with a geographical boundary of 34–41.5° (latitude) and 137–145° (longitude). Furthermore, three data subsets are defined based on the distribution of magnitude-distance criteria considered to have an adequate number of data in each dataset (Fig. 3b): MR1 corresponding to 166 entries with R = 20 ± 50% and M = 3.5 ± 0.5; MR2 corresponding to 575 entries with R = 120 ± 60% and M = 4.5 ± 0.5 and MR3 corresponding to 274 entries with R = 250 ± 70% and M = 5.5 ± 0.5). The distribution of PGA for MR1/MR2/MR3 is shown in Fig. 3c. Astorga et al. [20,21] analyzed the time variation of the resonance frequency of the ANX building since 1998. They defined four time periods corresponding to changes in its behavior. During the first period (T1), the fundamental frequency starts to decrease immediately after the completion of construction work, from 1998 to 2005. Frequency stabilizes during period T2 (2006–2011/02/30) until the Tohoku earthquake sequence in 2011. During period T3, the fundamental frequency drops significantly and a slow recovery of the resonance frequency is observed directly after the Tohoku earthquake during the immediate aftershock sequence between 2011/03/01 and 2011/09/30. Finally, T4 corresponds to the period between 2011/10/01 and 2018/05/15. T1/T2/T3/T4 comprise a total of 366/313/402/468 data, respectively. Four further subsets of data within the magnitude distance criteria MR2 are considered according to the period criteria: T1-MR2 (118 data), T2-MR2 (119 data), T3-MR2 (193 data), and T4-MR2 (121 data).

One method of obtaining P[EDP|IM] is to perform a series of non-linear dynamic analyses for a given structure and for a given series of earthquakes [4]. Another method is to perform regression between EDP and IM, knowing the probability distribution [7,29] for variability analysis. The degree of scattering around the fitted model represents the uncertainty of the EDP|IM model. To analyze EDP|IM uncertainty and testing efficiency and sufficiency of IMs, one-parameter log-log (log: natural logarithm) linear regression of EDP on IM [4] is used, defined as follows:

$$\log(EDP) = a + b.\, log(IM) + \varepsilon \tag{6}$$

where a and b are the estimated regression coefficients and ε is the standard error.

The variability associated with IMs and EDP is represented hereafter as σ_{IM}, and σ_{EDP}, respectively, i.e. the standard deviation of the log of IM and EDP values, normalized by their mean value.

The efficiency of IMs is defined simply as the IM that results in a small variability of EDP given IM [5]. The variability associated with EDP for a given IM is measured by calculating the standard deviation of the residuals of the fitted regression model between EDP and IM (Eq. (6)), represented hereafter as $\sigma_{EDP|IM}$. However, an efficient IM reduces the record-to-record variability between building responses. For practical purposes, this can then reduce the number of non-linear time history analyses for IDA [7] with the necessary degree of precision.

The sufficiency of IMs is defined as the IM that makes EDP conditionally independent on earthquake parameters such as magnitude (M) and source-to-site distance (R). Sufficiency is estimated by computing the linear regression between EDP and IM regression residuals (ε|IM) of Eq. (6) and the corresponding value of M or log(R) [5].

Fig. 4 shows the distribution of residual values EDP|PGA for the whole dataset, versus M or log(R). As expected, $\sigma_{EDP|PGA}$ varies significantly, reflecting several sources of uncertainties, which will be explored in the following section.

4. Results on EDP|IM

4.1. General trends - σ

For several candidate IMs, global and regional ground motion prediction equation (GMPE) models are continuously evolving [30]. For e.

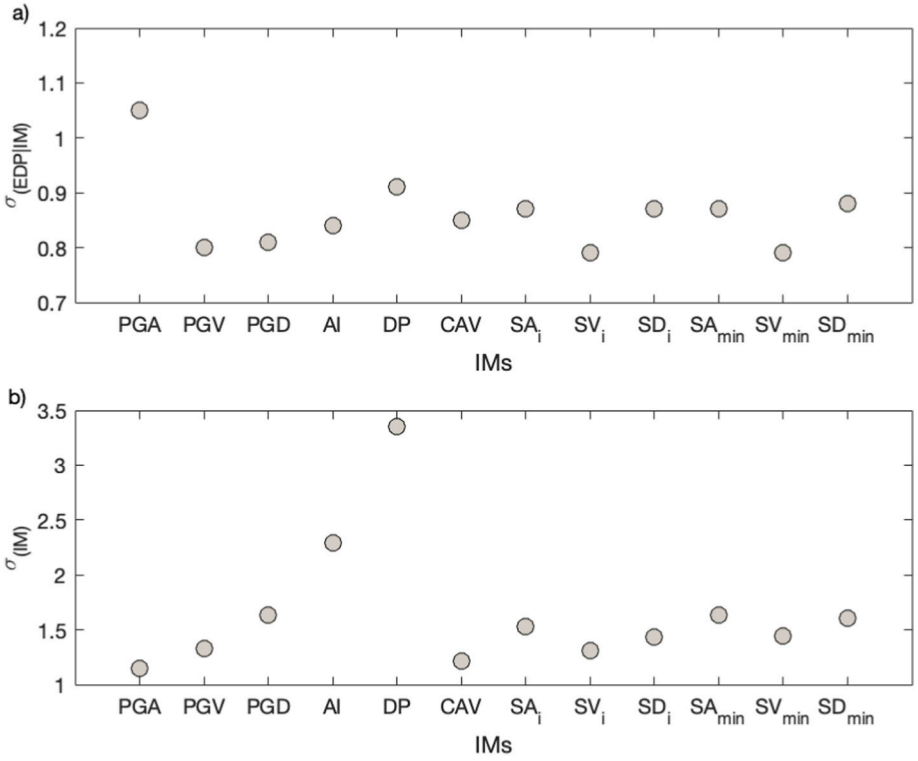

Fig. 5. (a) $\sigma_{EDP|IM}$ values for the IMs concerned, computed for the whole dataset. (b) σ_{IM} values.

g., Dhakal et al. [31], Podili and Raghukanth [32], and Zhao et al. [33] developed GMPE models for Japan, the value of sigma (σ_{GMPE}) reported in these models were 0.86 for PGA, 0.70 for PGV, 0.82 for PGD, 1.46 for AI, 0.69 for CAV, and 0.64–0.88 for acceleration response spectra, and 0.28–0.39 for velocity response spectra with a structural period ranging from 0.01 to 5 s. Atkinson [34] developed GMPE models for the US, the value of sigma reported for these models were 0.37 for PGA, 0.33 for PGV, and 0.31–0.41 for acceleration response spectra with a structural

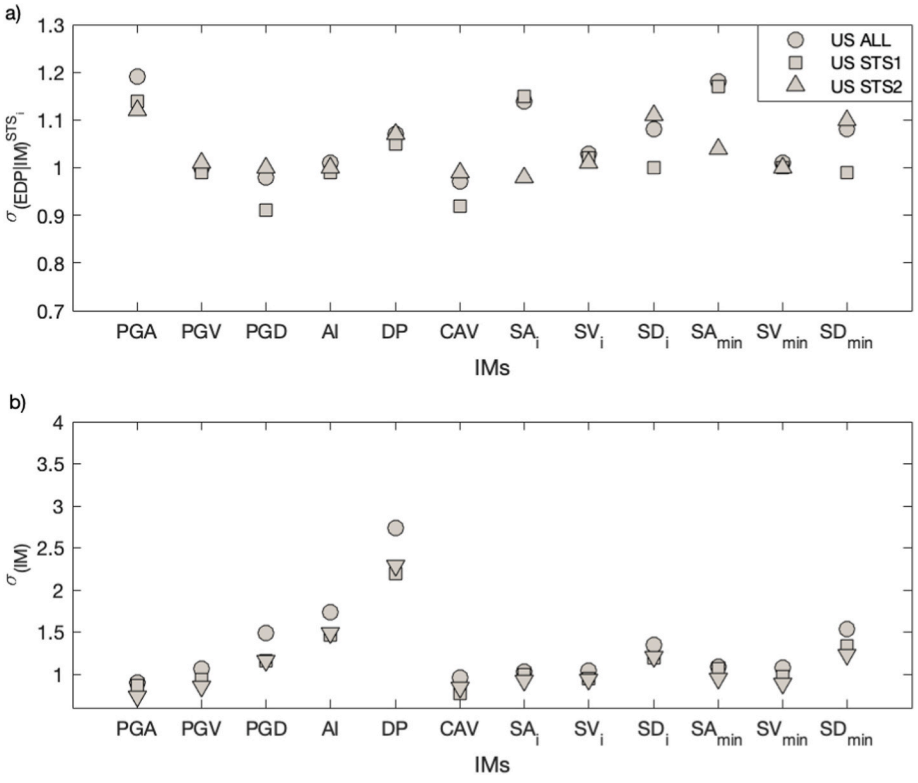

Fig. 6. (a) Values of $\sigma_{EDP|IM}$ for the IMs concerned computed for US buildings by tectonic region (US STS1 and US STS2) and for all US buildings (US ALL). (b) σ_{IM} values associated with each IM.

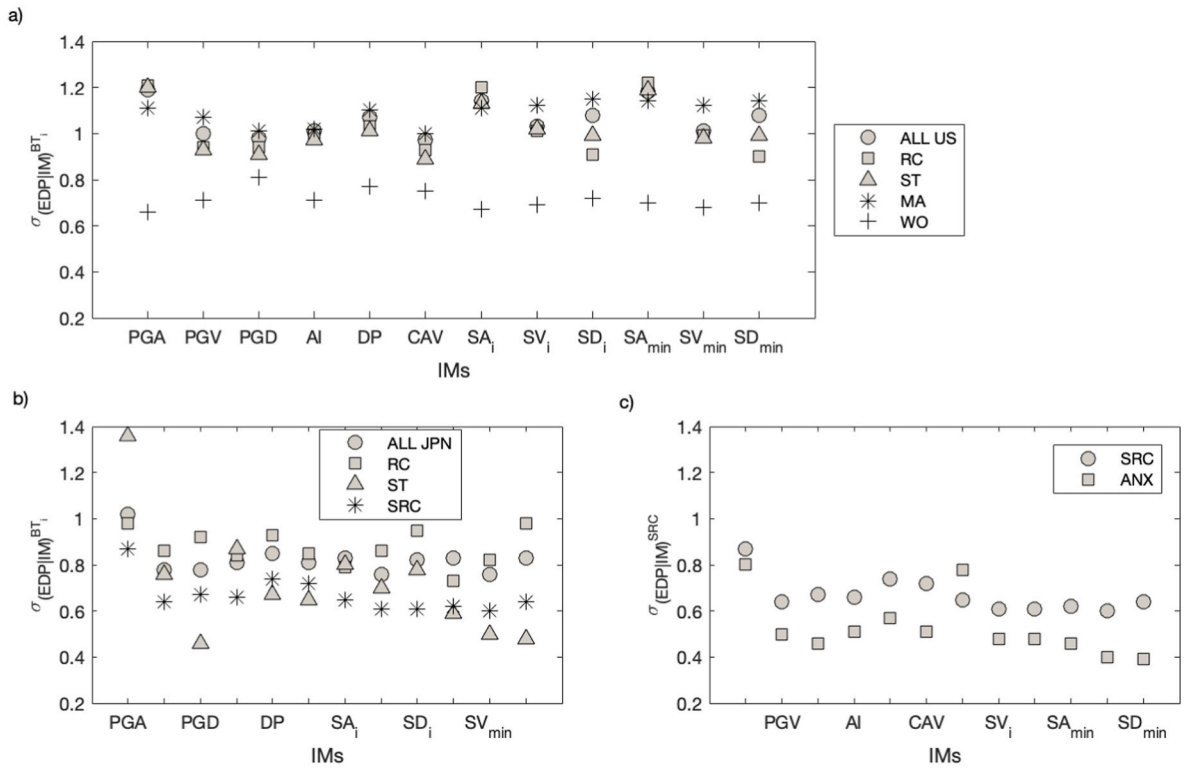

Fig. 7. Variability of $\sigma_{EDP|IM}$ values as a function of the class of buildings (a) US dataset, (b) JPN dataset, (c) ANX single building dataset.

period ranging between 0.03 and 5 s.

This section compares the efficiency of these candidates IMs in structural response prediction using our experimental data. Fig. 5 shows the standard deviation of the residuals of the fitted standard log-linear regression model between EDP and IM (Eq. (6)) for ALL (JPN + US + RO) datasets. For each IM parameter, σ_{IM} is given in Fig. 5b. All the σ_{EDP}, σ_{IM} and $\sigma_{EDP|IM}$ values are provided in Appendix A1. In the main body of the manuscript, only the most relevant results are discussed.

The first observation is that the JPN dataset ($\sigma_{EDP} = 1.44$), largest in terms of numbers, is predominant in our global dataset (1.48) compared with the US dataset (1.32). Fig. 5a shows that the value of $\sigma_{EDP|IM}$ is oscillating between 0.8 and 1.1, with an average value of 0.9. The highest value of $\sigma_{EDP|IM}$ corresponds to the spectral and peak ground acceleration values and DP intensity measures. Fig. 5b shows that PGA corresponds to the smallest value of σ_{IM} (1.15), whereas spectral acceleration corresponds to the highest value of σ_{IM} (in average around 1.60) after DP (3.33) and AI (2.29). Here we can see that the velocity related IMs (PGV, SV_i and SV_{min}) corresponds to the relatively smaller value of σ_{IM}. However, for AI and DP, $\sigma_{EDP|IM}$ remains similar to the other values. This indicates that these parameters are not good indicators of the natural variability of ground motion and do not enable a high degree of certainty for predicting the response of structures for a given IM.

In this study, the velocity related IMs are observed with a smaller value of $\sigma_{EDP|IM}$ (e.g., 0.80 for PGV, 0.79 for SV_i, and 0.79 for SV_{min}). The efficiency of velocity IMs has already been reported for US data by Perrault and Guéguen [19] and is confirmed herein, regardless of the dataset considered. It is interesting to note that these IMs are associated with the relatively smallest value of σ_{GMPE} in the above mentioned GMPE models, thus, the velocity related IMs are the most efficient IMs i.e. PGV, SV_i, and SV_{min}.

In order to capture the origins of the uncertainties in building response prediction, several relationships are tested in the following sections, according to tectonic region, building typology and ageing effect. The paucity of the data for specific analysis in some datasets makes it necessary to separate the studies; sub-datasets are therefore presented.

4.2. *Variability associated with the tectonic context - σ_R*

Atkinson and Morisson [35] demonstrated that seismic ground-motion amplitudes in northern and southern California were significantly different for the same magnitude/distance pair of earthquakes, without identifying the origin of this difference, but related to different tectonic regions. In this study, the effect of the region on building response is examined for all building classes. Fig. 6 shows the effect of the tectonic region on the US dataset. The whole US dataset (US ALL) and both STS1 and STS2 subsets are tested, considering all of the previously mentioned US building typologies. Note that for STS1 and STS2, the σ_{EDP} values are the same (1.24 and 1.20 respectively, Appendix A1), and σ_{IM} differs only marginally. In Fig. 6, the effect of considering the data by specific region barely minimizes the $\sigma_{EDP|IM}$ values, for the same values of σ_{IM} (Fig. 6b). Some exceptions should be noted, the most remarkable being displacement and acceleration. Firstly, the figure shows that for velocity IMs (i.e. PGV, SV_i and SV_{min}), the $\sigma_{EDP|IM}$ values are similar, being around 1 for ALL, STS1 and STS2 (values in Appendix A1). On the other hand, the $\sigma_{EDP|IM}$ values for STS1 and STS2, respectively, correspond to 1.15 and 0.97 for SA_i, 1.15 and 1.04 for SA_{min}, 1.03 and 1.10 for SD_i and 1.03 and 1.10 for SD_{min}. Thus, a trend inversion (the smallest values for STS2 or STS1) is observed depending on whether acceleration or displacement IM values are considered. Although the origin of this inversion has not been confirmed, the class of the buildings concerned in these two geographical areas is likely to be the cause, since some buildings are more sensitive to acceleration than others, depending on their period of resonance (i.e. stiff or flexible buildings). The following sections will therefore focus mainly on velocity IMs, testing the variability observed in relation to the class of structure in particular, and assuming an insignificant effect of the tectonic context.

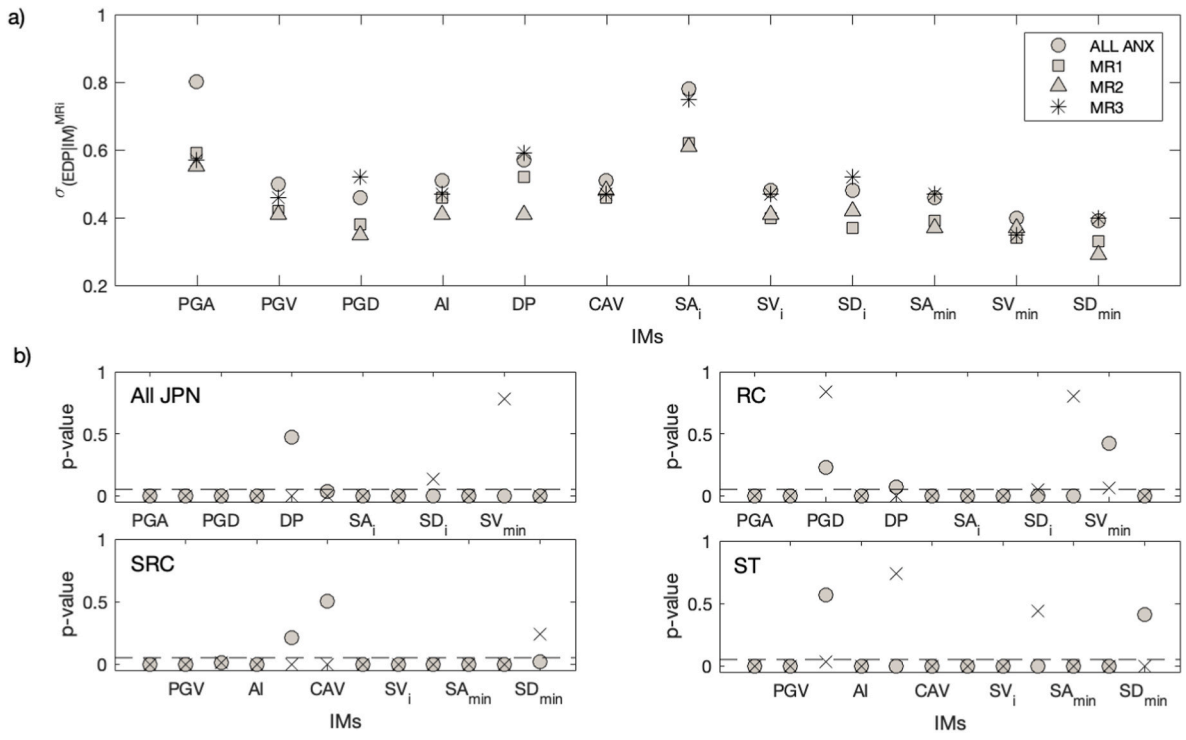

Fig. 8. (a) Variability of $\sigma_{EDP|IM}$ values as a function of the IMs concerned for different magnitude and earthquake-to-building distance criteria, considering the ANX single building dataset. Magnitude/distance criteria are R = 20 ± 50% and M = 3.5 ± 0.5 for MR1; R = 120 ± 60% and M = 4.5 ± 0.5 for MR2; R = 250 ± 70% and M = 5.5 ± 0.5 for MR3. (b) Sufficiency analysis with respect to magnitude (o) and distance (x) observed for the JPN building class datasets. The dashed line corresponds to a p-value of 0.05.

4.3. *Epistemic uncertainties related to building typology - σ_T*

The seismic performance of buildings depends on their design and characteristics (construction material, height, plan area, regularity etc.). The uncertainties affecting vulnerability assessments are mainly epistemic because, according to Spence et al. [36], they are due to the classification of buildings into typologies and the attribution of a single generic model to a whole class of buildings. Furthermore, when evaluating seismic capacity, we suppose that many buildings of the same typology have the same ergodic epistemic uncertainties, implying that the values of the epistemic uncertainties do not change between buildings. In this section, the variability associated with different classes of buildings is explored using the US and JPN datasets. Only a basic description of the buildings, based on material, is available in our database. A more detailed classification according to international standards (e.g., HAZUS typology, GEM taxonomy) could be considered in a more comprehensive analysis.

Fig. 7a shows the variability observed for different classes of buildings in the US dataset. The trends are the same as those observed previously between the velocity IMs and the other IMs. Two typologies stand out: MA and WO. For these two typologies, the small amount of data in our dataset does not allow a more detailed analysis nor a definitive conclusion as to the effectiveness of certain IMs for EDP prediction. However, for MA buildings, the velocity IMs give higher values of $\sigma_{EDP|IM}$, and IMs in acceleration and displacement seem more and less efficient, respectively, than for the other typologies, due to the greater stiffness (i.e. smaller resonance period) generally observed in such buildings. For WO, all the $\sigma_{EDP|IM}$ values are well below those of the other typologies, but the small number of buildings involved ultimately reduces the epistemic uncertainty related to structural differences within each building class.

For the US classes (Fig. 7a), the type of structure only has a slight influence on the $\sigma_{EDP|IM}$ values for the velocity IMs (i.e. 0.94 and 0.93 for PGV, 1.01 and 1.02 for SV_i, and 0.99 and 0.98 for SV_{min} for RC and ST, respectively, Appendix A1). On the other hand, a notable difference exists between US ST and US RC buildings in particular, the latter having a lower $\sigma_{EDP|IM}$ value for displacement IMs (i.e. 0.94 and 0.91 for PGD, 0.91 and 0.99 for SD_i for RC and ST buildings, respectively).

There are significant differences between the JPN data (Fig. 7b) and the US data. First of all, the velocity IMs give different $\sigma_{EDP|IM}$ values for different classes of buildings. For JPN ST, the $\sigma_{EDP|IM}$ values are all lower, reflecting lower epistemic uncertainty related to the diversity of buildings within this class; this contrasts with JPN RC buildings (e.g. 0.86 and 0.76 for PGV, 0.86 and 0.70 for SV_i and 0.82 and 0.50 for SV_{min} for JPN RC and JPN ST buildings, respectively). This epistemic uncertainty is confirmed in Fig. 7c, where the $\sigma_{EDP|IM}$ values for one specific single building (ANX building) are compared with those of its building class. There is a significant contribution to the specific single building $\sigma_{EDP|IM}$ values, with significantly reduced $\sigma_{EDP|IM}$ values (e.g., 0.64 to 0.50 for PGV, 0.61 to 0.48 for SV_i, and 0.60 to 0.40 for SV_{min}), particularly for parameters other than acceleration. It is also interesting to note an evident contribution of the response spectra calculated by taking into account the co-seismic response values to significantly reduce $\sigma_{EDP|IM}$ for the SRC buildings (e.g., 0.78/0.48/0.48 for $SA_i/SV_i/SD_i$ and 0.46/0.40/0.39 for $SA_{min}/SV_{min}/SD_{min}$ for the ANX building, Fig. 7c). Co-seismic resonance frequency, which modifies co-seismic demand, is known to vary for this building [20,21], as well as for a specific US ST building reported by Ref. [18]. A similar variation is observed for JPN ST buildings (Fig. 7b), significantly reducing the $\sigma_{EDP|IM}$ values (e.g., 0.80/0.70/0.78 for $SA_i/SV_i/SD_i$ and 0.59/0.50/0.48 for $SA_{min}/SV_{min}/SD_{min}$). This point will be analyzed more specifically in the last section of this manuscript.

4.4. *Within-building variability associated with earthquake magnitude-distance - σ_{MR}*

Fig. 8a shows the effect of M/R pairs on the variability of the ANX building response. The M/R criteria are described in Fig. 3 (section 3).

Table 1
p-values for the whole JPN dataset, and by JPN building class. Values in bold are greater than 0.05, i.e. the threshold for evaluating IM sufficiency.

		PGA	PGV	PGD	AI	DP	CAV	SA_i	SV_i	SD_i	SA_{min}	SV_{min}	SD_{min}
All JPN	M	0.00	0.00	0.00	0.00	**0.47**	0.03	0.00	0.00	0.00	0.00	0.00	0.00
	R	0.00	0.00	0.00	0.00	0.00	0.00	0.00	0.00	**0.13**	0.00	**0.78**	0.00
RC	M	0.00	0.00	**0.23**	0.00	**0.07**	0.00	0.00	0.00	0.00	0.00	**0.42**	0.00
	R	0.00	0.00	**0.84**	0.00	0.00	0.00	0.00	0.00	**0.05**	**0.80**	**0.06**	0.00
SRC	M	0.00	0.00	0.01	0.00	**0.21**	**0.50**	0.00	0.00	0.00	0.00	0.00	0.02
	R	0.00	0.00	0.01	0.00	0.00	0.00	0.00	0.00	0.00	0.00	0.00	**0.24**
ST	M	0.00	0.00	**0.57**	0.00	0.00	0.00	0.00	0.00	0.00	0.00	0.00	**0.41**
	R	0.00	0.00	0.03	0.00	**0.74**	0.00	0.00	0.00	**0.44**	0.00	0.00	0.00

Firstly, there is a significant effect on $\sigma_{EDP|IM}$ values compared with the totality of the ANX data, regardless of the IMs considered, except for the displacement values of the IMs for the MR3 data subset (R = 250 ± 70% and M = 5.5 ± 0.5). These events generated longer periods of ground motion, to which the ANX building, with its resonance period of around 1Hz [20], is more sensitive. For MR1 and MR2, the $\sigma_{EDP|IM}$ values are lower than the values of the ANX dataset, particularly for the velocity IMs (values for $PGV/SV_i/SV_{min}$ are 0.50/0.48/0.40 for all ANX data compared with 0.42/0.40/0.34 for MR1 and 0.41/0.41/0.37 for MR2) and for the displacement IMs (values for $PGD/SD_i/SD_{min}$ are 0.46/0.48/0.39 for all ANX data compared with 0.38/0.37/0.33 for MR1 and 0.35/0.42/0.29 for MR2).

IM sufficiency is tested by considering the JPN building class dataset. The statistical significance of the coefficient obtained from the standard linear regression for M and log(R) is assessed based on the p-value (i.e. the probability of obtaining an estimated value of the coefficient at least as large as the actual value, the actual value of the coefficient being zero) [37]. If the p-value observed is greater than or equal to 0.05, the estimated coefficient of M or log(R) is statistically insignificant and the IM is considered sufficient [5]. For the JPN building class, Fig. 8b shows the p-value considering all the IM parameters, summarized in Table 1.

Based on Fig. 8b, it appears difficult to conclude on the sufficiency of the IMs tested on our dataset, i.e. EDP is not conditionally independent of magnitude and distance. For the ALL-JPN dataset, the most sufficient IM with respect to magnitude is DP (p-value = 0.47) and with respect to distance SD_i (0.13) and SV_{min} (0.78), the latter value (the highest) allowing us to assume that the prediction of EDP knowing SV_{min} is statistically independent of distance. However, for individual building classes, the p-values differ between IMs. It seems that displacement IMs are the most sufficient in distance, such as PGD (p-value = 0.57) and SD_{min} (0.41) for the ST class, as these buildings are the most slender - long-period buildings, i.e. more sensitive to ground displacements. For RC buildings, the most sufficient IMs (in distance) are SA_{min} (p-value = 0.80) and PGD (0.84) and, to a lesser extent, SD_i (0.05) and SV_{min} (0.06). For the same class of buildings, the sufficient IMs in magnitude are SV_{min} (p-value = 0.42) and, to a lesser extent, PGD (0.23) and DP (0.07). Finally, for SRC buildings, only two IMs (DP and CAV) are sufficient in magnitude, with p-values of 0.21 and 0.50, respectively.

Since sufficiency differs according to building class, these results suggest that particular attention should be paid when selecting the accelerometric time histories used to perform non-linear time history analysis or PBEE assessment. Furthermore, if insufficient IMs are considered, site-specific ground motion data must be provided to avoid inaccurate estimation of the damage levels or failure rates used in PBEE if the ground motion characteristics do not match the source and site requirements [38].

4.5. Within-building variability associated with aging - σ_A

Karapetrou et al. [39] discussed the effect of aging over time on the seismic vulnerability of buildings. Moreover, Astorga et al. [20,21] demonstrated the time-dependent response of the ANX building to cumulative events during a long sequence of moderate to strong earthquakes in experimental conditions. Incorporating the real state of a structure may therefore help to reduce variability, yielding more reliable results for PBEE analysis. Fig. 9 shows the $\sigma_{EDP|IM}$ variations as a function of the age of the ANX building. Astorga et al. [20,21] distinguished four specific periods (T1 to T4) during which the frequency of the building changed over time, depending on structural health related to the cumulative damage in the structure. Astorga et al. [20,21] also showed that ANX's response between seismic events stabilized with its degradation, expressed as a function of the dispersion of structural drift values.

These four periods are considered here, focusing only on the M/R dataset corresponding to MR2 (i.e. the dataset with the most data). A progressive reduction of $\sigma_{EDP|IM}$ values is observed between T1 and T4, the last two periods being the most efficient (Appendix A1), which confirms the results previously reported in Astorga et al. [21] concerning the stability of the building response with degradation. It therefore appears that taking into account the ageing or actual state of a structure in performance analysis will help to modify the efficiency of the IMs, particularly as even moderate seismic shaking may change the building response [40]. For example, for $PGV/SV_i/SV_{min}$, the $\sigma_{EDP|IM}$ values correspond to 0.39/0.37/0.35 for the MR2-T2 ANX dataset and 0.37/0.37/0.26 for the MR2-T3 ANX dataset, compared with 0.41/0.41/0.37 for the MR2 ANX dataset as a whole. This results in a reduction of the performance prediction uncertainties as required during aftershock sequences for the short-time operative assessment of

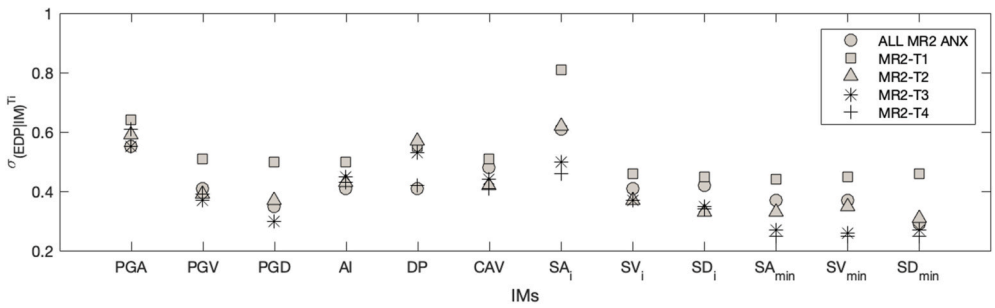

Fig. 9. Variation of $\sigma_{EDP|IM}$ values as a function of the IMs for different periods, considering seismic cumulative damage in the ANX building. Magnitude/distance criteria (MR2) are R = 120 ± 60% and M = 4.5 ± 0.5 and periods T1 to T4 are described in the manuscript.

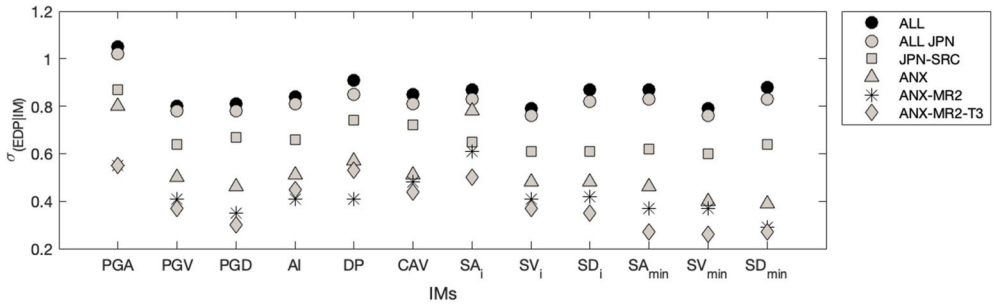

Fig. 10. Summary of the variation of $\sigma_{EDP|IM}$ values as a function of the IMs concerned, considering different components of the uncertainties in prediction models.

Table 2
Summary of the $\sigma_{EDP|IM}$ values and their reduction (in %) applied to the specific ANX building. The Avg column is the mean value of all IMs.

	PGA	PGV	PGD	AI	DP	CAV	SA_i	SV_i	SD_i	SA_{min}	SV_{min}	SD_{min}	Avg.
σ	1.05	0.80	0.81	0.84	0.91	0.85	0.87	0.79	0.87	0.87	0.79	0.88	**0.86**
σ_R	1.02	0.78	0.78	0.81	0.85	0.81	0.83	0.76	0.82	0.83	0.76	0.83	**0.82**
σ_R/σ	3%	3%	4%	4%	7%	5%	5%	4%	6%	5%	4%	6%	**4%**
σ_T	0.87	0.64	0.67	0.66	0.74	0.72	0.65	0.61	0.61	0.62	0.60	0.64	**0.67**
σ_T/σ_R	15%	18%	14%	19%	13%	11%	22%	20%	26%	25%	21%	23%	**19%**
σ_B	0.80	0.50	0.46	0.51	0.57	0.51	0.78	0.48	0.48	0.46	0.40	0.39	**0.53**
σ_B/σ_T	8%	22%	31%	23%	23%	29%	−20%	21%	21%	26%	33%	39%	**21%**
σ_{MR}	0.55	0.41	0.35	0.41	0.41	0.48	0.61	0.41	0.42	0.37	0.37	0.29	**0.42**
σ_{MR}/σ_B	31%	18%	24%	20%	28%	6%	22%	15%	13%	20%	8%	26%	**19%**
σ_A	0.55	0.37	0.30	0.45	0.53	0.44	0.50	0.37	0.35	0.27	0.26	0.27	**0.39**
σ_A/σ_{MR}	0%	10%	14%	−10%	−29%	8%	18%	10%	17%	27%	30%	7%	**8%**
σ_A/σ	48%	54%	63%	46%	42%	48%	43%	53%	60%	69%	67%	69%	**55%**

time-dependent building capacity assessment, based on resonance period shift [41,42].

5. Summary

Fig. 10 is a summary of the identification of building response prediction uncertainties for the different IMs considered, based on available data and metadata. In general, for the specific case of the ANX building, the $\sigma_{EDP|IM}$ values are considerably lower than the model evaluated on the dataset to take into account structural characteristics such as construction type or ageing. For example, for $PGV/SV_i/SV_{min}$, the $\sigma_{EDP|IM}$ values decrease from 0.41/0.41/0.37 to 0.37/0.37/0.26. Table 2 summarizes the contribution of each component to the epistemic uncertainties of Eq. (6). While the regional distinction (σ_R) does not bring any significant gain (4% on average), distinction by type of construction (σ_T) and specific building (σ_B) contributes significantly (19% and 21% respectively). Concerning the IMs that make EDP conditionally independent from magnitude M and source-to-site distance (σ_{MR}), the figure shows that all the IMs are globally non-sufficient, with a reduction of $\sigma_{EDP|IM}$ values of approximately 19% for the specific case of the ANX building. When ageing (σ_A), i.e. the actual health of the structure, is taken into account, the $\sigma_{EDP|IM}$ values are reduced by 8%.

In total, the spectral IMs benefit most from these successive components. For example, the $SA_{min}/SV_{min}/SD_{min}$ value reductions are equal to 69%/67%/69% for $\sigma_{EDP|IM}$ values corresponding to 0.27/026/0.27. These results concern one specific building, with a resonance frequency of approximately 1 Hz. For longer- or shorter-resonance period buildings, the results would be different, particularly for acceleration or displacement IM values. However, spectral values integrating the co-seismic increase of the resonant period (index *min*) allow a reduction of the $\sigma_{EDP|IM}$ values of approximately 10%.

5.1. Building frequency variation and the average response spectral value as an IM

Many previous studies [18,20,21,28,43–47] have observed the co-seismic shifting of the resonance frequency for different building typologies. Using a US dataset, Perrault and Guéguen [19] showed that mean spectral values computed between the pre- and co-seismic periods provided the most effective IM for the EDP|IM model. On the other hand, several authors [9,10,12,38,48–51] investigated the average spectral values computed between two periods to take into account the co-seismic nonlinear response of building in structural analysis. All these studies were carried using numerical modeling. Boomer et al. [48] considered the correlation of damage measures and average spectral IMs computed between T1 and F*T1, T1 being the elastic period of structure, for F values from 1.7 to 3. Bianchini et al. [10] found the most efficient and sufficient spectral values computed from 0.2*T1 to 2*T1 and 0.2*T1 to 3*T1. Eads et al. [12] concluded that average spectral acceleration computed between 0.2*T1 and 3*T1 yields lower variability in terms of structural response. Ebrahimian et al. [9] also considered three average spectral values between 0.2*T1 and 1.5*T1, T1 and 2*T1, and 0.2*T1

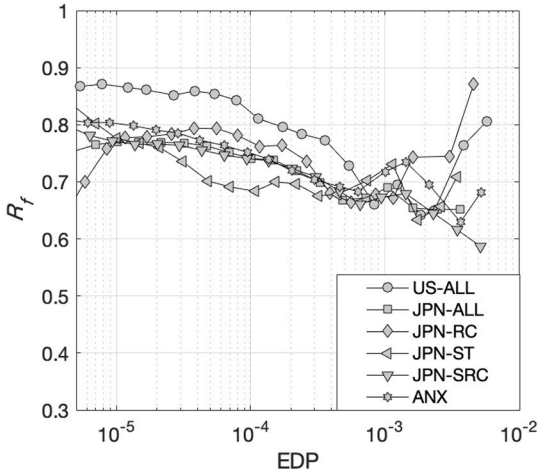

Fig. 11. Variation of the frequency ratio (R_f=f_{min}/f_i) for different datasets.

Table 3
Empirical building damage prediction model according to building class.

IM	Parameter	BT-ALL	BT-RC	BT-SRC	BT-ST	BT-MA	BT-WO
SV_{min}	a	−10.22	−10.65	−10.00	−9.81	−9.17	−9.26
	b	0.87	0.83	0.89	1.08	0.55	0.58
	σ	0.79	0.84	0.60	0.60	1.10	0.68
PGV	a	−9.41	−9.78	−9.21	−9.17	−8.80	−9.02
	b	0.94	0.86	0.95	1.16	0.60	0.55
	σ	0.80	0.87	0.64	0.80	1.07	0.71

and 2*T1. Adam et al. [49] used average spectral acceleration values computed from T1 to 1.6*T1 and from 0.2*T1 to 1.6*T1 and observed a reduction of dispersion in the collapse capacity relationship. Finally, Kohrangi et al. [50,51] observed that the average spectral acceleration value from 0.2 T1 to 1.5 T1 yields better prediction of structural response. We found no clear consensus on the values to be considered to reproduce co-seismic demand in structure analysis.

In this study, the frequency variation with respect to EDP was observed for the JPN dataset by building class. Fig. 11 summarizes the variation of the frequency ratio $R_f = f_{min}/f_i$ between pre-seismic frequency (f_i) and co-seismic frequency f_{min} with respect to EDP for different JPN building classes and the whole US database, with EDP ranging from 5 10^{-6} to 10^{-2}. The variation of R_f confirms that, regardless of building class, the frequency shift between the pre- and the co-seismic period increases with EDP, which means large frequency drops occur for the strongest earthquakes. Significant variation of R_f is observed even at the lower end of the EDP range from 0.9 to 0.65 (below the slight damage threshold = 0.0025). For EDP values between 10^{-5} and 10^{-3}, a relatively similar trend is observed regardless of building class, with R_f values decreasing from 0.78 to 0.65. There are no stronger earthquakes, which prevent us from extending this result to a higher level of drift, but this first experimental evaluation suggests the need to collect a large amount of earthquake data in buildings in order to refine our performance prediction models.

6. Conclusions

Experimental data is very useful in helping us to understand the complex physical processes at work in civil engineering structures to be able to integrate them into our models to reduce the epistemic uncertainty of these complex process. Earthquake data collected from buildings under long-term monitoring in Japan, the US and Romania were used to attempt to identify the components of the uncertainties associated with EDP|IM. Region-to-region, building-to-building and within-building uncertainties associated with earthquake magnitude-distance and ageing were explored.

Compared with the conventional IMs based on peak values or conventional spectral value (SA_i, SV_i or SD_i), the ground motion intensity measure, denoted SA_{min}, SV_{min} and SD_{min}, which considers inelastic period lengthening, was found to be the most efficient IM for estimating EDP, taken as structural drift herein. In terms of sufficiency, generally speaking, it appears that no IMs are sufficient due to a significant conditional dependence of EDP on R (i.e. earthquake source-to-building distance) and M (i.e. magnitude). Some exceptions are pointed out in Fig. 8 for specific building classes and IMs. In fact, depending on the type of building and, in particular, its period, displacement and acceleration IMs might be more efficient or sufficient; this could be confirmed with additional data and a specific analysis of the building characteristics, which is not considered by this study. Nevertheless, all our results indicate that velocity IMs are those that provide the lowest variability for predicting EDP given IM.

Based on the ANX building results, the components that make the largest contribution to overall uncertainties are building class and specific building associated with the M/R condition (Fig. 10, Table 2). When analyzing specific buildings using long-term monitoring data, the real structural state also appears to make a significant contribution to the uncertainties, reflecting the real co-seismic demand in EDP prediction. The underlying key issue is related to the variation of frequency, which is strongly dependent on EDP. Note that regardless of building class, this frequency variation follows the same trend for all the drift values in our dataset.

Several numerical studies have been carried out to investigate the efficiency and sufficiency of IMs considering one building or a group of buildings and using suits of input ground motions [8–16]. In contrast, this study compares the efficiency and sufficiency of IMs and the variation of sigma in the EDP|IM relationship using real experimental data. We are able to capture the real structural response from different building typologies during several earthquakes, which is the main advantage of this study. This study shows that the most commonly used IMs i.e. PGA and SA_i are not efficient and sufficient to predict the structural response within the range of our dataset. The velocity related IMs i.e., PGV, SV_i, and SV_{min} are observed to be the most efficient in building response prediction. Our findings strongly agree with previous studies carried out on real data by Perrault and Guéguen [19]. It is very interesting note here that the IMs which are found efficient in our studies are also associated with relatively smaller variability in the available GMPE models.

This study highlights the importance of real experimental dataset. Having more information on the earthquakes and descriptions of the building characteristics would help to improve the prediction of structural response for analyzing seismic vulnerability or loss assessment. Although the amount of data contained in our dataset provides relevant results, the paucity of data concerning specific classes of buildings or components of uncertainties limits the strength of the conclusions that can be drawn. To resolve outstanding issues, we must continue our international collaborative efforts and motivate building owners to share their data, which would increase their interest in this type of study. In particular, having more specific data would enable verification of the aforementioned conclusions.

Moreover, building response prediction models can be developed considering several parameters related to earthquakes and buildings, such as ground motion IM, magnitude, distance, building typology, height, structural properties, etc. [19,52,53]. In conclusion to this study, an empirical building damage prediction model is proposed (Table 3) based on the entire dataset (US, Japan and Romania) according to building class and considering the most efficient IMs (SV_{min} and PGV) using the functional form given in Eq. (6):

$$\log(\mathrm{EDP}) = \mathrm{a} + \mathrm{b}.\ \log(\mathrm{IM}) + \varepsilon$$

Author statement

Subash Ghimire: Conceptualization, Methodology, data preparation, Investigation, Visualization, writing-draft preparation. Philippe Guéguen: Conceptualization, Investigation, Visualization, Supervision, Writing – review & editing. Ariana Astorga: Conceptualization, data preparation, reviewing and editing.

Declaration of competing interest

The authors declare that they have no known competing financial

interests or personal relationships that could have appeared to influence the work reported in this paper.

Acknowledgments

This work is part of the URBASIS program led by P.G at ISTerre/ Université de Grenoble Alpes. Japanese data were obtained from the BRI Strong Motion Observation (http://smo.kenken.go.jp/). US data were provided by the Center for Engineering Strong Motion Data (CESMD, https://strongmotioncenter.org/). Romanian data were obtained from the National Center for Seismic Risk Reduction (NCSRR, http://cnrrs.utcb.ro/cnrrs_en/). P.G. would like to thank LabEx OSUG@2020 (Investissements d'avenir-ANR10LABX56). S.G. would like to thank the ITN-MSCA URBASIS project, a project funded by the EU Horizon 2020 program under Grant Agreement Number 813137. This project is part of the Real-time Earthquake Risk Reduction for a Resilient Europe 'RISE' project that has received funding from the European Union's Horizon 2020 research and innovation programme under grant agreement No 821115..

Appendix A. Supplementary data

Supplementary data to this article can be found online at https://doi.org/10.1016/j.soildyn.2021.106751.

Appendix

Table A1

σ_{IM}, σ_{EDP}, and $\sigma_{EDP|IM}$ values considering different sub datasets discussed in the manuscript

			PGA	PGV	PGD	AI	DP	CAV	SA_i	SV_i	SD_i	SA_{min}	SV_{min}	SD_{min}
US + JPN + RO	ALL	IM	1.15	1.33	1.63	2.29	3.35	1.21	1.53	1.31	1.43	1.63	1.44	1.61
		EDP	1.48	1.48	1.48	1.48	1.48	1.48	1.48	1.48	1.48	1.48	1.48	1.48
		EDP|IM	1.05	0.80	0.81	0.84	0.91	0.85	0.87	0.79	0.87	0.87	0.79	0.88
US data	ALL	IM	0.90	1.07	1.49	1.73	2.73	0.96	1.03	1.04	1.35	1.09	1.08	1.54
		EDP	1.32	1.32	1.32	1.32	1.32	1.32	1.32	1.32	1.32	1.32	1.32	1.32
		EDP|IM	1.19	1.00	0.98	1.01	1.07	0.97	1.14	1.03	1.08	1.18	1.01	1.08
	STS1	IM	0.86	0.94	1.15	1.48	2.20	0.77	1.00	1.06	1.20	1.03	1.08	1.31
		EDP	1.24	1.24	1.24	1.24	1.24	1.24	1.24	1.24	1.24	1.24	1.24	1.24
		EDP|IM	1.14	1.00	0.93	1.00	1.07	0.93	1.15	1.03	1.03	1.15	1.01	1.03
	STS2	IM	0.74	0.85	1.15	1.49	2.29	0.84	0.92	0.95	1.20	0.95	0.92	1.29
		EDP	1.20	1.20	1.20	1.20	1.20	1.20	1.20	1.20	1.20	1.20	1.20	1.20
		EDP|IM	1.12	1.01	0.99	1.00	1.06	0.98	0.97	1.01	1.10	1.04	1.01	1.10
	RC	IM	0.84	0.98	1.47	1.58	2.63	0.91	1.03	1.03	1.25	1.07	1.04	1.31
		EDP	1.32	1.32	1.32	1.32	1.32	1.32	1.32	1.32	1.32	1.32	1.32	1.32
		EDP|IM	1.21	0.94	0.94	0.99	1.03	0.93	1.20	1.01	0.91	1.22	0.99	0.90
	ST	IM	0.84	1.01	1.46	1.55	2.78	0.87	0.91	1.02	1.32	0.99	1.08	1.64
		EDP	1.28	1.28	1.28	1.28	1.28	1.28	1.28	1.29	1.28	1.28	1.29	1.28
		EDP|IM	1.20	0.93	0.91	0.97	1.01	0.89	1.13	1.02	0.99	1.19	0.98	0.99
	MA	IM	0.91	1.08	1.43	1.83	2.35	1.02	0.94	1.27	1.71	1.00	1.18	1.46
		EDP	1.23	1.23	1.23	1.23	1.23	1.23	1.23	1.21	1.21	1.23	1.23	1.23
		EDP|IM	1.11	1.07	1.01	1.02	1.10	1.00	1.11	1.12	1.15	1.14	1.12	1.14
	WO	IM	1.02	1.36	1.83	2.20	3.21	1.21	1.07	1.32	1.60	1.06	1.32	1.65
		EDP	1.02	1.02	1.02	1.02	1.02	1.02	1.02	1.02	1.02	1.02	1.02	1.02
		EDP|IM	0.66	0.71	0.81	0.71	0.77	0.75	0.67	0.69	0.72	0.70	0.68	0.70
Japanese	ALL	IM	1.11	1.31	1.61	2.26	3.34	1.22	1.50	1.30	1.42	1.61	1.43	1.61
		EDP	1.44	1.44	1.44	1.44	1.44	1.44	1.44	1.44	1.44	1.44	1.44	1.44
		EDP|IM	1.02	0.78	0.78	0.81	0.85	0.81	0.83	0.76	0.82	0.83	0.76	0.83
	RC	IM	0.98	1.13	1.50	2.02	2.98	1.12	1.25	1.09	1.22	1.37	1.20	1.35
		EDP	1.28	1.28	1.28	1.28	1.28	1.28	1.28	1.28	1.28	1.28	1.28	1.28
		EDP|IM	0.98	0.86	0.92	0.84	0.93	0.85	0.79	0.86	0.95	0.73	0.82	0.98
	SRC	IM	1.14	1.40	1.66	2.36	3.53	1.24	1.48	1.37	1.46	1.56	1.52	1.68
		EDP	1.48	1.48	1.48	1.48	1.48	1.48	1.48	1.48	1.48	1.48	1.48	1.48
		EDP|IM	0.87	0.64	0.67	0.66	0.74	0.72	0.65	0.61	0.61	0.62	0.60	0.64
	ST	IM	1.11	1.24	1.61	2.18	3.24	1.21	1.72	1.37	1.56	1.65	1.43	1.70
		EDP	1.67	1.67	1.67	1.67	1.67	1.67	1.67	1.67	1.67	1.67	1.67	1.67
		EDP|IM	1.36	0.76	0.46	0.87	0.67	0.65	0.80	0.70	0.78	0.59	0.50	0.48
ANX building	ALL	IM	1.00	1.27	1.51	2.12	3.25	1.13	1.54	1.31	1.42	1.44	1.41	1.59
		EDP	1.42	1.42	1.42	1.42	1.42	1.42	1.42	1.42	1.42	1.42	1.42	1.42
		EDP|IM	0.80	0.50	0.46	0.51	0.57	0.51	0.78	0.48	0.48	0.46	0.40	0.39
	STS	IM	1.01	1.28	1.50	2.13	3.25	1.13	1.55	1.32	1.43	1.45	1.42	1.60
		EDP	1.43	1.43	1.43	1.43	1.43	1.43	1.43	1.43	1.43	1.43	1.43	1.43
		EDP|IM	0.80	0.50	0.45	0.50	0.56	0.50	0.78	0.48	0.47	0.45	0.39	0.39
	MR1	IM	0.69	0.80	0.90	1.30	2.10	0.65	1.06	0.85	0.91	0.89	0.88	0.97
		EDP	0.86	0.86	0.86	0.86	0.86	0.86	0.86	0.86	0.86	0.86	0.86	0.86
		EDP|IM	0.59	0.42	0.38	0.46	0.52	0.46	0.62	0.40	0.37	0.39	0.34	0.33
	MR2	IM	0.71	0.75	0.78	1.16	1.82	0.57	1.21	0.79	0.89	0.89	0.79	0.86
		EDP	0.71	0.71	0.71	0.71	0.71	0.71	0.71	0.71	0.71	0.71	0.71	0.71
		EDP|IM	0.55	0.41	0.35	0.41	0.41	0.48	0.61	0.41	0.42	0.37	0.37	0.29
	MR3	IM	0.79	0.86	0.96	1.47	2.17	0.73	1.10	0.85	0.93	0.88	0.92	1.03
		EDP	1.02	1.02	1.02	1.02	1.02	1.02	1.02	1.02	1.02	1.02	1.02	1.02
		EDP|IM	0.57	0.46	0.52	0.47	0.59	0.47	0.75	0.47	0.52	0.47	0.35	0.40
	T1-MR2	IM	0.83	0.95	1.02	1.58	2.19	0.81	1.18	0.92	0.99	0.98	0.98	1.05

(continued on next page)

Table A1 (*continued*)

		PGA	PGV	PGD	AI	DP	CAV	SA_i	SV_i	SD_i	SA_{min}	SV_{min}	SD_{min}
	EDP	0.94	0.94	0.94	0.94	0.94	0.94	0.94	0.94	0.94	0.94	0.94	0.94
	EDP|IM	0.64	0.51	0.50	0.50	0.55	0.51	0.81	0.46	0.45	0.44	0.45	0.46
T2-MR2	IM	0.66	0.77	0.89	1.24	1.93	0.61	1.17	0.86	0.94	0.86	0.84	0.90
	EDP	0.85	0.85	0.85	0.85	0.85	0.85	0.85	0.85	0.85	0.85	0.85	0.85
	EDP|IM	0.59	0.39	0.37	0.43	0.57	0.42	0.62	0.37	0.33	0.33	0.35	0.31
T3-MR2	IM	0.60	0.71	0.80	1.14	1.98	0.57	0.91	0.78	0.82	0.79	0.80	0.90
	EDP	0.80	0.80	0.80	0.80	0.80	0.80	0.80	0.80	0.80	0.80	0.80	0.80
	EDP|IM	0.55	0.37	0.30	0.45	0.53	0.44	0.50	0.37	0.35	0.27	0.26	0.27
T4-MR2	IM	0.63	0.75	0.90	1.22	2.13	0.61	0.98	0.83	0.87	0.91	0.89	1.01
	EDP	0.80	0.80	0.80	0.80	0.80	0.80	0.80	0.80	0.80	0.80	0.80	0.80
	EDP|IM	0.61	0.39	0.30	0.43	0.42	0.41	0.46	0.37	0.34	0.25	0.25	0.25

References

[1] Porter K. An overview of PEER's performance-based earthquake engineering methodology. Proc. ninth Int. Conf. Appl. Stat. Probab. Civ. Eng. (ICASP9), San Fr. 2003.
[2] Baker JW, Cornell CA. Uncertainty propagation in probabilistic seismic loss estimation. Struct Saf 2008;30:236–52. https://doi.org/10.1016/j.strusafe.2006.11.003.
[3] Iervolino I. Assessing uncertainty in estimation of seismic response for PBEE. Earthq Eng Struct Dynam 2017;46:1711–23. https://doi.org/10.1002/eqe.2883.
[4] Luco N. Probabilistic seismic demand analysis, SMRF connection fractures, and near-source effects. Dep Civ Environ 2002:260.
[5] Luco N, Cornell CA. Structure-specific scalar intensity measures for near-source and ordinary earthquake ground motions. Earthq Spectra 2007;23:357–92.
[6] Baker JW, Cornell CA. Vector-valued intensity measures for pulse-like near-fault ground motions. Eng Struct 2008;30:1048–57. https://doi.org/10.1016/j.engstruct.2007.07.009.
[7] Shome N, Cornell CA. Probabilistic seismic demand analysis of nonlinear structures. Reliability of marine structures program report No. RMS-35. California: Dept. of Civil and Environmental Engineering, Stanford University; 1999. http://pitch.stanford.edu/rmsweb/Thesis/NileshShome.pdf.
[8] Buratti N. A comparison of the performances of various ground–motion intensity measures. In: 15th world conf. Earthq. Eng. Lisbon. .: Port; 2012. p. 77.
[9] Ebrahimian H, Jalayer F, Lucchini A, Mollaioli F, Manfredi G. Preliminary ranking of alternative scalar and vector intensity measures of ground shaking. Bull Earthq Eng 2015;13:2805–40. https://doi.org/10.1007/s10518-015-9755-9.
[10] Bianchini M, Diotallevi PP, Baker JW. Prediction of inelastic structural response using an average of spectral accelerations. In: 10th international conference on structural safety and reliability (ICOSSAR09), vol. 1317; 2009. p. 8.
[11] Lin L, Naumoski N, Saatcioglu M, Foo S. Improved intensity measures for probabilistic seismic demand analysis. part 1: development of improved intensity measures. Can J Civ Eng 2011;38:79–88. https://doi.org/10.1139/L10-110.
[12] Eads L, Miranda E, Lignos D. Average spectral acceleration as an intensity measure for collapse risk assessment. Earthq Eng Struct Dynam 2015;44:2057–73. https://doi.org/10.1002/eqe.
[13] Jayaram N, Lin T, Baker JW. A Computationally efficient ground-motion selection algorithm for matching a target response spectrum mean and variance. Earthq Spectra 2011;27:797–815. https://doi.org/10.1193/1.3608002.
[14] Mollaioli F, Silvia B, Luis D, Rodolfo S. Correlations between energy and displacement demands for performance-based seismic engineering. Pure Appl Geophys 2011;168:237–59. https://doi.org/10.1007/s00024-010-0118-9.
[15] Luco N, Manuel L, Baldava S, Bazzurro P. Correlation of damage of steel moment-resisting frames to a vector-valued set of ground motion parameters. In: Proc 9th Int Conf Struct Saf Reliab; 2005. p. 2719–26.
[16] Vamvatsikos D, Cornell CA. Developing efficient scalar and vector intensity measures for IDA capacity estimation by incorporating elastic spectral shape information. Earthq Eng Struct Dynam 2005;34:1573–600. https://doi.org/10.1002/eqe.496.
[17] Trifunac MD, Todorovska MI, Manić MI, Bulajić BĐ. Variability of the fixed-base and soil–structure system frequencies of a building—the case of Borik-2 building. Struct Control Heal Monit Off J Int Assoc Struct Control Monit Eur Assoc Control Struct 2010;2:15–120. https://doi.org/10.1002/stc.
[18] Guéguen P, Johnson P, Roux P. Nonlinear dynamics induced in a structure by seismic and environmental loading. J Acoust Soc Am 2016;140:582–90. https://doi.org/10.1121/1.4958990.
[19] Perrault M, Guéguen P. Correlation between ground motion and building response using California earthquake records. Earthq Spectra 2015;31:2027–46. https://doi.org/10.1193/062413EQS168M.
[20] Astorga A, Guéguen P, Kashima T. Nonlinear elasticity observed in buildings during a long sequence of earthquakes. Bull Seismol Soc Am 2018;108:1185–98. https://doi.org/10.1785/0120170289.
[21] Astorga AL, Guéguen P, Rivière J, Kashima T, Johnson PA. Recovery of the resonance frequency of buildings following strong seismic deformation as a proxy for structural health. Struct Health Monit 2019;18:1966–81. https://doi.org/10.1177/1475921718820770.
[22] Astorga A, Guéguen P, Ghimire S, Kashima T. NDE1.0: a new database of earthquake data recordings from buildings for engineering applications. Bull Earthq Eng 2020;18:1321–44. https://doi.org/10.1007/s10518-019-00746-6.
[23] Arias A. Measure of earthquake intensity: Massachusetts inst. of tech. Santiago de Chile: Cambridge. Univ. of Chile; 1970.
[24] Araya R, Saragoni GR. Earthquake accelerogram destructiveness potential factor. Pap. Present. Proc. 8th World Conf. Earthq. Eng. 1984:7.
[25] Epri A. Criterion for determining expedience of the operating basis earthquake. Palo Alto, California: Electric Power Research Institute, prepared by Jack R: Benjamin and Associates, Inc; 1988.
[26] Auger F, Flandrin P. Improving the readability of T-F and T-S by reassignment Method.pdf. IEEE Trans Signal Process May 1995 1995;43(No 5):1068–89. 43.
[27] Kashima T. Dynamic behavior of an eight-storey SRC building examined from strong motion records. Pap. Present. 13th World Conf. Earthq. Eng. 2004.
[28] Kashima T. Dynamic behaviour of src buildings damaged by the 2011 great east Japan earthquake based on strong motion records. Second Eur Conf Earthq Eng Seismol 2014:1–11.
[29] Cornell CA, Luco N. The effect of connection fractures on steel moment resisting frame seismic demands and safety. 1999.
[30] Douglas J. Ground motion prediction equations 1964-2020. 2020.
[31] Dhakal YP, Takai N, Sasatani T. Empirical analysis of path effects on prediction equations of pseudo-velocity response spectra in northern Japan. Earthq Eng Struct Dynam 2008;39:443–61. https://doi.org/10.1002/eqe.952.
[32] Podili B, Raghukanth STG. Ground motion prediction equations for higher order parameters. Soil Dynam Earthq Eng 2019;118:98–110. https://doi.org/10.1016/j.soildyn.2018.11.027.
[33] Zhao JX, Jiang F, Shi P, Xing H, Huang H, Hou R, et al. Ground-motion prediction equations for subduction slab earthquakes in Japan using site class and simple geometric attenuation functions. Bull Seismol Soc Am 2016;106:1535–51. https://doi.org/10.1785/0120150056.
[34] Atkinson GM. Ground-motion prediction equation for small-to-moderate events at short hypocentral distances, with application to induced-seismicity hazards. Bull Seismol Soc Am 2015;105:981–92. https://doi.org/10.1785/0120140142.
[35] Atkinson GM, Morrison M. Observations on regional variability in ground-motion amplitudes for small-to-moderate earthquakes in North America. Bull Seismol Soc Am 2009;99:2393–409. https://doi.org/10.1785/0120080223.
[36] Spence R, Bommer J, Del Re D, Bird J, Aydinoğlu N, Tabuchi S. Comparing loss estimation with observed damage: a study of the 1999 Kocaeli earthquake in Turkey. Bull Earthq Eng 2003;1:83–113. https://doi.org/10.1023/A:1024857427292.
[37] Benjamin JR, Cornell CA. Solutions manual to accompany probability, statistics and decision for civil engineer. McGraw-Hill; 1970.
[38] Kazantzi AK, Vamvatsikos D. Intensity measure selection for vulnerability studies of building classes. Earthq Eng Struct Dynam 2015;44:2677–94. https://doi.org/10.1002/eqe.2603.
[39] Karapetrou S, Manakou M, Bindi D, Petrovic B, Pitilakis K. "Time-building specific" seismic vulnerability assessment of a hospital RC building using field monitoring data. Eng Struct 2016;112:114–32. https://doi.org/10.1016/j.engstruct.2016.01.009.
[40] Perrault M, Guéguen P, Parra G, Sarango J. Modification of the data-driven period/height relationship for buildings located in seismic-prone regions such as Quito (Ecuador). Bull Earthq Eng 2020. https://doi.org/10.1007/s10518-020-00840-0.
[41] Trevlopoulos K, Guéguen P, Helmstetter A, Cotton F. Earthquake risk in reinforced concrete buildings during aftershock sequences based on period elongation and operational earthquake forecasting. Struct Saf 2020;84:101922. https://doi.org/10.1016/j.strusafe.2020.101922.
[42] Trevlopoulos K, Guéguen P. Period elongation-based framework for operative assessment of the variation of seismic vulnerability of reinforced concrete buildings during aftershock sequences. Soil Dynam Earthq Eng 2016;84:224–37. https://doi.org/10.1016/j.soildyn.2016.02.009.
[43] Mucciarelli M, Masi A, Gallipoli MR, Harabaglia P, Vona M, Ponzo F, et al. Analysis of RC building dynamic response and soil-building resonance based on data recorded during a damaging earthquake (Molise, Italy, 2002). Bull Seismol Soc Am 2004;94:53–1943. https://doi.org/10.1785/012003186.

[44] Calvi G, Pinho R, Crowley H. State-of-the-knowledge on the period elongation of RC buildings during strong ground shaking. First Eur Conf Earthq Eng Seismol 2006;3–8.
[45] Clinton JF, Bradford SC, Heaton TH, Favela J. The observed wander of the natural frequencies in a structure. Bull Seismol Soc Am 2006;96:237–57. https://doi.org/10.1785/0120050052.
[46] Masi A, Vona M. Experimental and numerical evaluation of the fundamental period of undamaged and damaged RC framed buildings. Bull Earthq Eng 2010;8:643–56. https://doi.org/10.1007/s10518-009-9136-3.
[47] Michel C, Gueguen P. Time-frequency analysis of small frequency variations in civil engineering structures under weak and strong motions using a reassignment method. Struct Health Monit 2010;9:159–71. https://doi.org/10.1177/1475921709352146.
[48] Bommer JJ, Magenes G, Hancock J, Penazzo P. The influence of strong-motion duration on the seismic response of masonry structures. Bull Earthq Eng 2004;2:1–26. https://doi.org/10.1023/B:BEEE.0000038948.95616.bf.
[49] Adam C, Kampenhuber D, Ibarra LF, Tsantaki S. Optimal spectral acceleration-based intensity measure for seismic collapse assessment of P-delta vulnerable frame structures. J Earthq Eng 2017;21:1189–95. https://doi.org/10.1080/13632469.2016.1210059.
[50] Kohrangi M, Bazzurro P, Vamvatsikos D. Vector and scalar IMs in structural response estimation, Part II: building demand assessment. Earthq Spectra 2016;32:1525–43. https://doi.org/10.1193/053115EQS081M.
[51] Kohrangi M, Bazzurro P, Vamvatsikos D, Spillatura A. Conditional spectrum-based ground motion record selection using average spectral acceleration. Earthq Eng Struct Dynam 2017;46(10):16.
[52] Fema F. 343: case studies-an assessment of the NEHRP guidelines for the seismic rehabilitation of buildings. 1999.
[53] Hancock J, Bommer JJ, Stafford PJ. Numbers of scaled and matched accelerograms required for inelastic dynamic analyses. Earthq Eng Struct Dynam 2008;14:1585–607.